ARTICLE

Preparation and Characterization of Transparent Polymeric Electrolyte Containing Ionic Liquid with Long Alkyl Chains for Electroactive Polymers

Received 00th January 20xx,
Accepted 00th January 20xx

DOI: 10.1039/x0xx00000x

Yuqing Dong[a], Ka-Wai Yeung[a], Chak-Yin Tang[a*], Chi Ho Wong[a], Wing-Cheung Law[a], Gary Chi-Pong Tsui[a], Xiaolin Xie[b]

Transparent polymer electrolytes are important components in fabricating transparent ionic electroactive polymers (iEAPs). Ionic liquids (ILs) have been widely used as the ionic source for polymeric electrolytes due to their broad electrochemical window and non-volatility. ILs with long alkyl chains, such as 1-decyl-3-methylimidazolium chloride (C_{10}MIMCl), may reduce the crystallinity and allow higher transparency of polymer electrolytes. However, it has been reported that the strong ionic interaction in C_{10}MIMCl hinders the migration of ions and thus affects the electromechanical deformation of polymer/C_{10}MIMCl electrolytes. In our work, iEAPs made of PVA/C_{10}MIMCl electrolytes were fabricated with high optical transparency. The poor electromechanical deformation of the electrolyte containing the long alkyl chain IL has been overcome. The hydrogen bonding formed between the IL cations ($C_{10}MIM^+$) and the polymer chains enabled the Cl^--controlled deformation. In addition, the hygroscopicity of IL allows for a higher degree of ion dissociation while the absorbed water widens the migration channels for Cl^-, and the combined effect has significantly improved the actuation performance of the iEAPs. We also found that the deformation of PVA/C_{10}MIMCl iEAPs increases with higher water content in the electrolyte, achieving the highest average bending curvature of $40.53 \pm 0.21\ m^{-1}$ under 2V DC. Compared with the iEAPs using the same IL reported in the literature, the actuation response of the iEAP containing C_{10}MIMCl is improved.

1 Introduction

Design and fabrication of optically transparent stimuli-responsive materials are important for developing advanced smart devices, such as zoom lenses, smart wipers, electronic skin, and environment-adaptive devices. Ionic electroactive polymers (iEAPs) [1-5] are promising candidates in fabricating transparent actuators and sensors due to the flexibility, safety, and remote-controllability. Once a potential (3~5V) is applied, iEAPs manifest bending deformation which is related to the directional movement of ions in the polymeric electrolytes [4-7]. However, transparent iEAPs are rarely reported owing to limited materials selection and difficulties in controlling the crystallization of the polymer matrices.

Transparent polymeric electrolytes are crucial in fabricating high-performance transparent iEAPs. Such electrolytes consist of polymers and ions, and possibly solvents. Commonly used polymers include proton exchange membranes, poly(vinylidene fluoride) (PVDF) with its copolymers, polydimethylsiloxane (PDMS), and polyvinyl alcohol (PVA). The choice of ions is more diverse, such as H^+, alkali metal ions, and organic cations. Although these materials are transparent, reduced crystallinity of crystalline polymers and good compatibility between the polymers and ions are necessary to realize high transparency in polymeric electrolytes [6].

In recent years, ionic liquids (ILs), especially imidazole-type ILs, have been widely used as the ionic source in fabricating iEAPs due to their thermal and chemical stability, as well as non-volatility [8-10]. A large number of studies have reported that using ILs can effectively reduce the crystallinity and thus increase the amorphous phase and enhance the flexibility of polymers, facilitating larger deformation of the iEAPs [11-13]. Compared with other ILs, imidazolium chloride ILs at the same mass fraction provide polymers with better electrical properties and more flexibility [14]. However, small deformation and back-relaxation may occur when ILs are introduced into polymeric electrolytes [15-17]. To improve the deformation of the IL-based iEAPs, adjusting the ILs concentration or type, introducing additional mobile ions such as Li^+, and generating ions migration channels have been reported [9, 15, 18]. Despite the large variety of ILs, only ILs with short alkyl chains, i.e. the number of side-chain carbons being less than 4, are commonly used. From a theoretical point of view, using larger ions is more advantageous for iEAP deformation [19, 20].

[a] Department of Industrial and Systems Engineering, The Hong Kong Polytechnic University, Hong Kong, China
[b] School of Chemistry and Chemical Engineering, Huazhong University of Science and Technology, Wuhan, Hubei 430074, China
† Footnotes relating to the title and/or authors should appear here.

In addition, polymers complexed with longer alkyl chains ILs exhibit more uniform grain size and lower crystallinity which allows higher transparency [14]. However, ILs with longer alkyl chains may inhibit the actuation performance of iEAPs due to the low ion-exchange capacity [15, 21-23] or cations mobility [18, 24]. Fabrication of transparent and high-performance iEAPs based on ILs with long alkyl chains is still an uphill struggle [13]. Adopting the single-ion controlled bending mechanism is one of the approaches to enhance the electromechanical response of iEAPs [25]. In this case, significant electrochemical performance can be achieved even with small ions such as Li^+ [26]. However, it is challenging to realize a similar mechanism using ILs with longer alkyl chains due to the weak coupling between the ILs anion and polymer [27], as well as the increased ionic interaction with the larger cation alkyl chain length [28, 29].

In this work, an IL with long alkyl chains, C_{10}MIMCl, and PVA were used to prepare highly transparent electrolytes for iEAPs, and single-ion controlled deformation was successfully achieved. The high transparency originates from the good compatibility between PVA and IL, as well as the reduced crystallinity of the polymer. The chloride ion-controlled actuation deformations resulted from the formation of hydrogen bonding between the IL cations and the PVA chains. In addition, owing to the hygroscopicity of IL [30, 31], water absorbed by the IL facilitates its dissociation and provides migration channels for the ions. The influences of IL and water content in the electrolytes on the mechanical and electromechanical properties were studied. It was found that the flexibility of the polymeric electrolytes is enhanced with higher IL and water content. At the same water content, the highest bending curvature of iEAP can be optimized at a particular IL content, while at the same IL content, a higher water content stimulates larger deformation. This approach allows the batch fabrication of transparent electrolytes, laying the foundation for the further fabrication of transparent high-performance iEAPs. In addition, due to the loading of the IL, the PVA/IL transparent electrolytes show considerable potential in the preparation of separators for capacitors and cells, and smart materials related to dehumidification and humidity monitoring.

2 Experimentation

2.1 Materials

Polyvinyl alcohol (PVA, polymerization degree 1750±50), ionic liquid (1-Decyl-3-methylimidazolium Chloride, C_{10}MIMCl), and the gold foil (thickness, 100±10 nm) were purchased from Sinopharm Group Co. Ltd (China), Aladdin, and Ouci Metal, respectively. All the materials were used as received.

2.2 Preparation of PVA/IL electrolytes and iEAPs

PVA/IL electrolytes: IL of the corresponding mass was dissolved in distilled water, forming a homogeneous solution, after which PVA was added to prevent salting out. The mixed solution in a sealed container was then heated to 95°C in an oil bath with vigorous stirring to dissolve the PVA. To remove any bubbles, the PVA/IL solution was cooled down and kept at room temperature for at least 24 h. The PVA/IL electrolytes were fabricated by casting the solution in a petri dish. To avoid the acetal reactions among the PVA chains [32], the evaporation of the water was carefully controlled at room temperature under atmospheric pressure. Due to the inherent hygroscopicity of IL and good compatibility with PVA, the as-fabricated electrolytes were hydrated and remained transparent. The water content was calculated by the following equation.

$$\textbf{Water content} = \frac{m_2 - m_1}{m_2} \times 100\% \quad (1)$$

where m_1 is the total mass of PVA and IL in the casting solution, and m_2 is the mass of the PVA/IL electrolyte. The electrolytes with different water content were prepared by moisture absorption from the environment and vacuum drying at room temperature. The mass fractions of the PVA/IL solution and the final water content in the electrolytes are listed in Table 1. The hygroscopic property of the IL was also investigated by monitoring the mass of pristine IL every 2-3 days at room temperature.

PVA/IL iEAPs: gold foil supported by wax paper was first trimmed to the size of the target iEAP, and then attached to the top and bottom surfaces of the PVA/IL electrolyte. Through electrostatic adsorption, the gold foil can become well attached to the electrolyte without additional pressing. The positions of the gold foil electrodes on both sides were connected to an external voltage source. When a voltage is applied, the electrical transport of ions within the PVA/IL electrolyte is activated by the electric field, resulting in electromechanical deformation. Finally, the PVA/IL iEAP was obtained by cutting off the excess electrolyte. The size of the iEAP was 30 mm × 2 mm (length × width).

2.3 Characterization of the PVA/IL electrolytes and iEAPs

2.3.1 PVA/IL electrolytes

An FT-IR Spectrometer (Bruker Vertex-70) equipped with an ATR (attenuated total reflectance) internal reflection system was employed to characterize the interaction between the PVA and IL (C_{10}MIMCl). The FT-IR spectra were recorded with a resolution of 4 cm^{-1} in the transmittance mode over the wavelengths from 4000 to 475 cm^{-1}. The top surface and the fracture surface morphology of the

Table 1. Compositions of the PVA/IL solutions and electrolytes

Samples		PVA	PL5-1	PL5-2.5	PL5-5	PL5-7.5	PL5-10
PVA/IL casting solution	PVA (wt.%)	5					
	IL (wt.%)	0	1	2.5	5	7.5	10
PVA/IL electrolyte	PVA (wt.%)	100	82.27	60.24	44.97	35.98	30.29
	IL (wt.%)	0	8.62	29.90	44.89	54.47	60.43
	Water (wt.%)	0	9.11	9.86	10.14	9.55	9.28
	Thickness (μm)	75±5					

PVA/IL electrolytes were investigated by Field emission scanning electron microscopy (FE-SEM).

DSC (Mettler Toledo) was applied to characterize the thermodynamic behaviour of the PVA/IL electrolytes and measure the crystallinity. DSC testing was conducted in an N_2 atmosphere from -25°C to 200°C at a heating rate of 25 °C min^{-1}. The crystallinity (X_c) of the PVA in the polymeric electrolyte was calculated as follows:

$$X_c = (\frac{\Delta H_m}{\Delta H_m^0}) \times 100\% \quad (2)$$

where ΔH_m is the crystallization melting enthalpy of the PVA/IL electrolyte measured in the DSC curve, and $\Delta H_m^0 = 138.6\, Jg^{-1}$ is the theoretical melting enthalpy of 100% crystalline PVA [33]. All samples were dehydrated under vacuum at room temperature before the ATR-FTIR, and DSC characterizations.

To further investigate the enhancement of C_{10}MIMCl on the flexibility of the PVA, a universal testing machine (INSTRON 3344) was used to analyse the tensile strength and elongation at the breaking point of the PVA and the PVA/IL electrolytes. The stretching rate of each sample was 15 mm min^{-1}. The water content in the samples was controlled by static water absorption or vacuum drying at room temperature. The effects of the IL concentration and water content in the electrolytes on flexibility are discussed.

A UV-Vis spectrophotometer (Ocean Optics) was used to measure the transparency of the PVA/IL electrolytes within the wavelengths from 200 nm to 800 nm.

2.3.2 PVA/IL iEAPs

It has been reported that there is a positive correlation between the capacitance and the actuation performance of iEAPs [34-36]. Therefore, the electrochemical properties of the PVA/IL iEAP were examined through the cyclic voltammetry (CV) method using a potentiostat (PAARSTAT 2263). A two-electrode configuration was adopted. Each iEAP was rested for 60 seconds before the measurement. The applied potential was swept at a rate of 50 mV s^{-1} within the range -0.5 to +0.5V. A total of 7 cycles were undertaken for each sample, and to ensure reproducibility, the scan data in the last cycle was selected to calculate the capacitance (C) of the iEAP by the following equation:

$$C = \frac{1}{2\Delta U v}\int_{V_0}^{V_0+\Delta U} IdV \quad (3)$$

where ΔU is the potential range, v is the scan rate, and V_0 is the minimum voltage during the CV test.

The actuation performance of the as-fabricated iEAP was evaluated based on the method previously reported by our group, which is related to the average curvature and the variation in curvature (i.e. curvature profile) of a sample with length L [37]. The iEAP was placed in cantilever mode to reduce the influence of gravity on the bending performance. To record the electromechanical response, we built an experimental setup to measure the bending profile of the iEAP. The schematic diagram is shown in Figure 1. Copper clips were used in contact with the gold electrodes to fix the iEAP at one end. The free-end length of iEAP was 20 mm. The camera lens was placed above the iEAP sample. The out-of-plane direction of the iEAP and the reference grids were parallel to each other. A DC voltage of 2V was applied, and the bending profile of iEAP was recorded. We tuned the physical properties and the composition of the materials so as to make the iEAP more flexible. The average curvature results were calculated by using three set of samples.

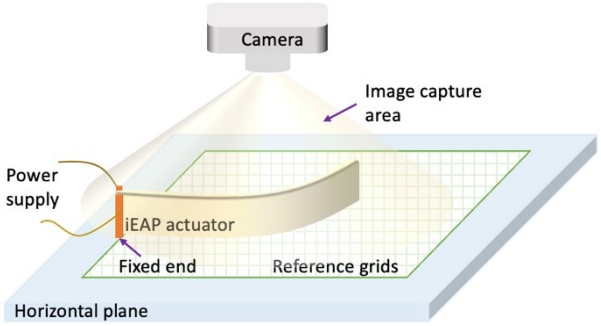

Figure 1. A schematic diagram of image acquisition of iEAP actuation

3 Results and discussion

3.1 Characterizations of the PVA/IL electrolytes

The FT-IR spectra of the IL, PVA membrane, and PVA/IL electrolytes are shown in Figure 2. After adding IL, the spectra of the electrolytes and the PVA matrix are not superimposed on each other but are related to the interaction between IL and PVA [38]. When compared to the spectral characteristic peaks of the PVA membrane, the H-C-N bending mode of the imidazole ring at 1178 cm^{-1} can be found in all PVA/IL electrolytes [39]. When the IL content is increased, hydrogen bonds between the cis-second amides (3151 cm^{-1}) and =C-H (3092 cm^{-1}) may be formed [38, 40]. As observed, the vibrational stretching mode of the hydroxyl group on the PVA chain at 3245 cm^{-1} shifts and strengthens gradually with increasing IL content. The -OH stretching mode shifts to 3351 cm^{-1} in sample PL5-10. The shift is probably due to the hydrogen bonds formed between the cation of IL and PVA, as agreed with the ref. [38] and [41]. The formation of hydrogen bonds is beneficial in controlling the migration of certain ions and presumably actuates the bending performance of the iEAP.

When compared to IL, the C-Cl stretching mode [42] at 757 cm^{-1} disappears in electrolytes PL5-1 and PL5-2.5. As proof, the IL is completely dissociated if it is less concentrated than PVA. On the other hand, the cations in IL can form a carbene structure in the absence of the C-H bending mode of the imidazole ring at 728 cm^{-1} along the out-of-plane direction, and the C-H bending mode in the methyl group at 1126 cm^{-1} [38]. The C-Cl stretching mode is observed in PL5-7.5 and PL5-10, indicating that the excess ions reassemble into neutral molecules in these PVA/IL electrolytes.

Further, the intensity of the methylene group (2856 cm^{-1}) and methine group (2915 cm^{-1}) in the polymer chains, as well as the swing mode of the backbone chain (-CH at 843 cm^{-1}) increases with the IL content. This is ascribed to a large number of methylene and methine groups contained in the IL cations. A more concentrated IL triggers a stronger intensity of -CH deformation mode at 1417 cm^{-1}. Moreover, the intensity of the -OH bending mode of PVA at 916 cm^{-1} is inversely proportional to the IL content, which indicates the existence of O-N interaction [43]. The C=N tensile mode at 1560 cm^{-1} and the C=C & C=N bending modes at 1645 cm^{-1} of the imidazole ring is more pronounced with increased IL content. In addition, a high concentration of IL actuates the formation of possible complexation of the hydroxyl and carbene at 1640 cm^{-1}, which is further evidenced of the interaction between the PVA and IL [38]. When the IL content

is higher, the intensity of the crystalline peak of PVA at 1142 cm^{-1} is lowered, and the non-crystalline peak at 1093 cm^{-1} is more noticeable in Figure 2 [44]. In addition, no peaks were observed at around 1720-1740 cm^{-1} and 2650-2880 cm^{-1} for the formation of aldehyde, suggesting no acetal reaction occurred during the electrolyte preparation.

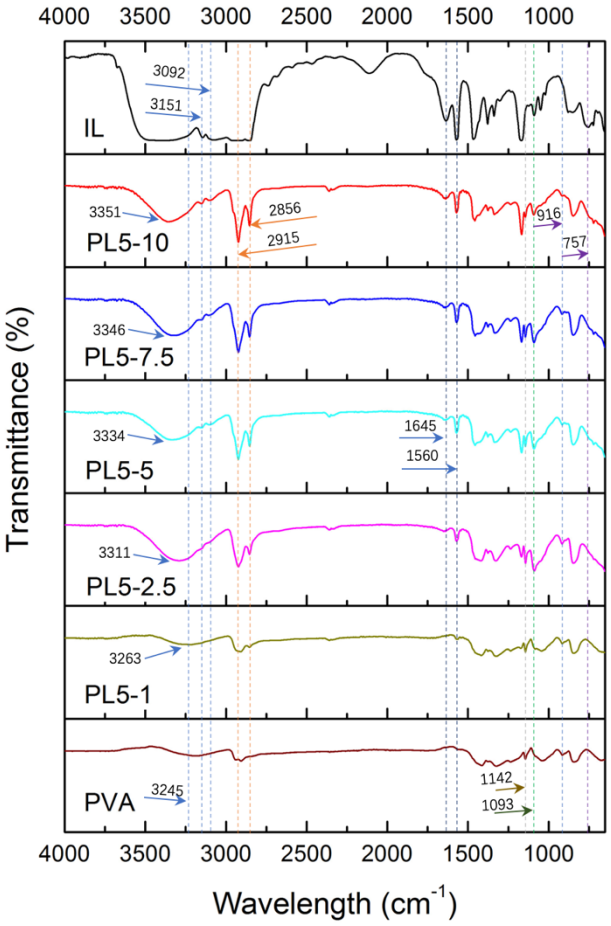

Figure 2. ATR-FTIR of IL, PVA membrane, and the PVA/IL electrolytes

The process of fabricating PVA/IL electrolyte and hydrogen bond formation between PVA and IL cations, as well as the anion-controlled bending performance of iEAP are shown in Figure 3. The bulky imidazolium cation in IL can readily form a stable nitrogen heterocyclic carbene [45], which is detached from the partial bonding due to the preliminary deprotonation. It can interact with the hydroxyl group on the PVA chain to form partial hydrogen bonds. Therefore, the cation is connected to the backbone of the PVA, and the actuation may originate from the migration of the Cl^-, manifesting a deformation towards its cathode side. Due to the good compatibility between the PVA and C_{10}MIMCl, the interplanar spacing of PVA is increased and the hydrogen bonds between molecular chains are weakened. Thus, the crystallinity of PVA is reduced by adding IL [46]. In addition, the C_{10}MIMCl penetrates the crystalline and amorphous regions of the polymer matrix. This result is further confirmed by the DSC characterization.

The good compatibility of the PVA and IL is further confirmed by the morphology of the electrolytes. Figure 4 shows the top surface and fracture surface images for the PVA/IL electrolytes samples (PVA, PL5-5, and PL5-10). Dense, non-porous, and homogeneous morphology is observed for all the samples. More importantly, no phase separation is observed, providing good evidence for the good compatibility of PVA and IL at these compositions.

3.2 Thermal and mechanical properties of the PVA/IL electrolytes

Figure 5(a) depicts the DSC curves (second heating) of the PVA and the PVA/IL electrolytes with different IL content. PVA is a polyhydroxylated and semi-crystalline polymer with strong intramolecular and intermolecular hydrogen bonds in which the melting point (T_m) is as high as 164°C. Thus, ions require more space or channels to move when PVA is used for iEAP, and the inhibition of ILs on PVA crystallization has been reported [47, 48]. On one hand, ILs provide mobile ions to deform the PVA-based iEAP more easily. On the other hand, the decreased crystallinity would accommodate

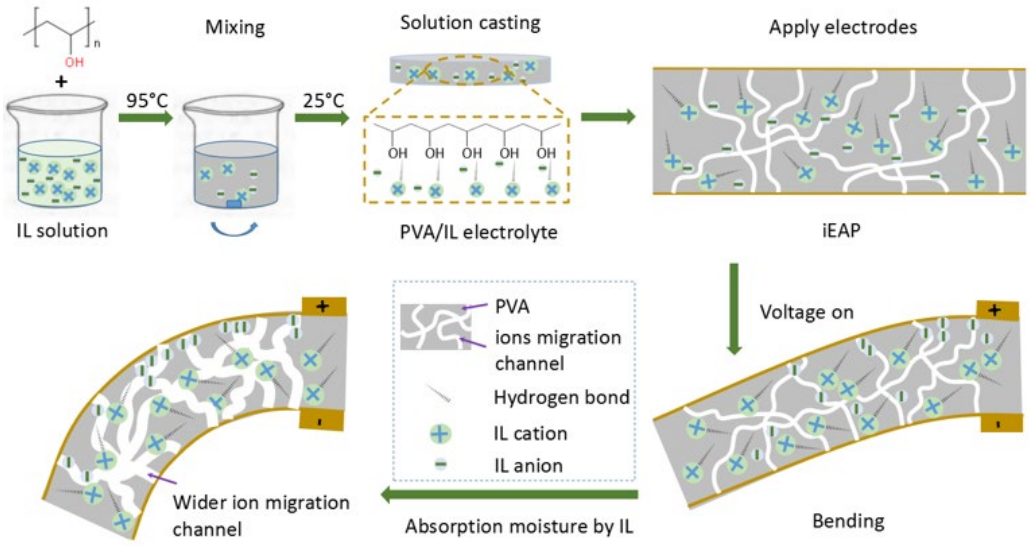

Figure 3. Illustration of the fabrication of PVA/IL electrolyte and formation of hydrogen bonding between PVA and IL, and the actuation mechanism of the PVA/IL iEAP

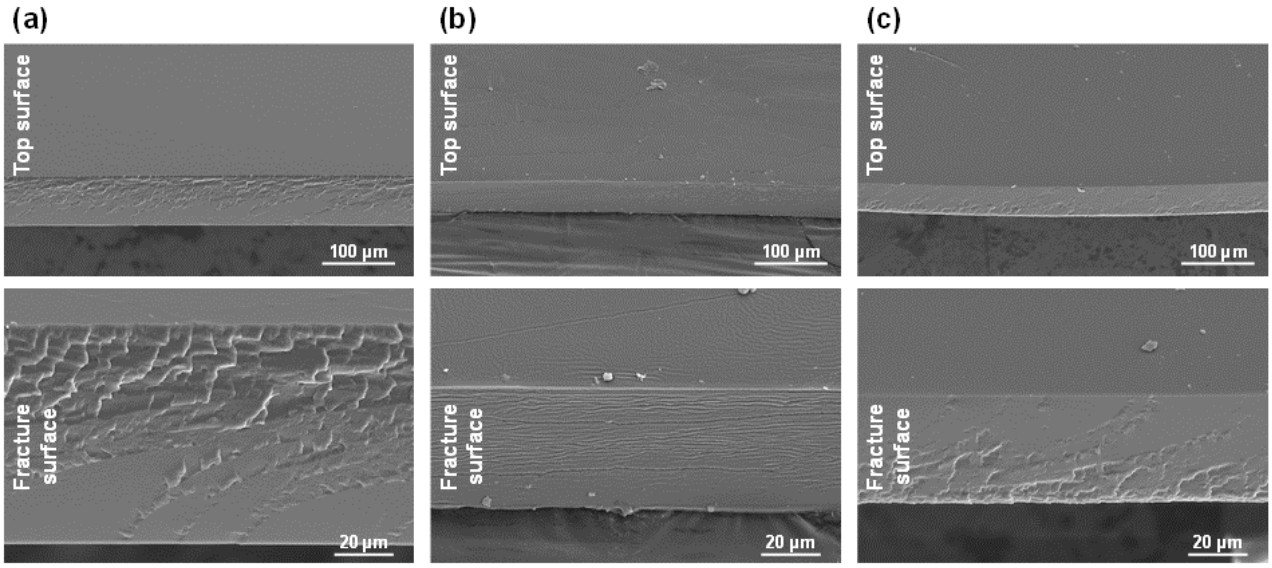

Figure 4. FE-SEM images of the top surface (upper one) and fracture surface (lower one) for (a) PVA, (b) PL5-5, and (c) PL5-10

more mobile ions and enhance the flexibility of the PVA, resulting in a superior actuation performance. As observed from the DSC results, only one melting peak is observed in each electrolyte at the beginning, indicating good compatibility between the IL and the PVA matrix at different mass fractions. With a higher IL content, the melting peak of the electrolytes becomes less pronounced, and the T_m is lowered. The crystallinity of the PVA membrane is 8.91%, while the lowest crystallinity is only 1.47% in PL5-10. This is due to a phenomenon in which the newly formed hydrogen bonds between the PVA and IL weaken the hydrogen bonds between hydroxyl groups on the PVA chains. Bending performance controlled by anions is always achievable whenever the kinematics of the cation is weak. Based on the results of ATR-FTIR and DSC, some probable interactions between the PVA and IL improve the flexibility of the PVA/IL electrolytes. The iEAP with softer electrolytes has been reported to exhibit a better bending performance [13].

As shown in Figure 5(b), the tensile behavior of the PVA membrane shows a classic stress-strain relationship (black line) of polymers. We observe that the membrane first undergoes elastic deformation, followed by a yield zone, a strain hardening zone, and finally, a fracture zone. The highest tensile modulus (0.779 GPa), breaking stress (0.042 GPa), and the lowest elongation at the breaking point

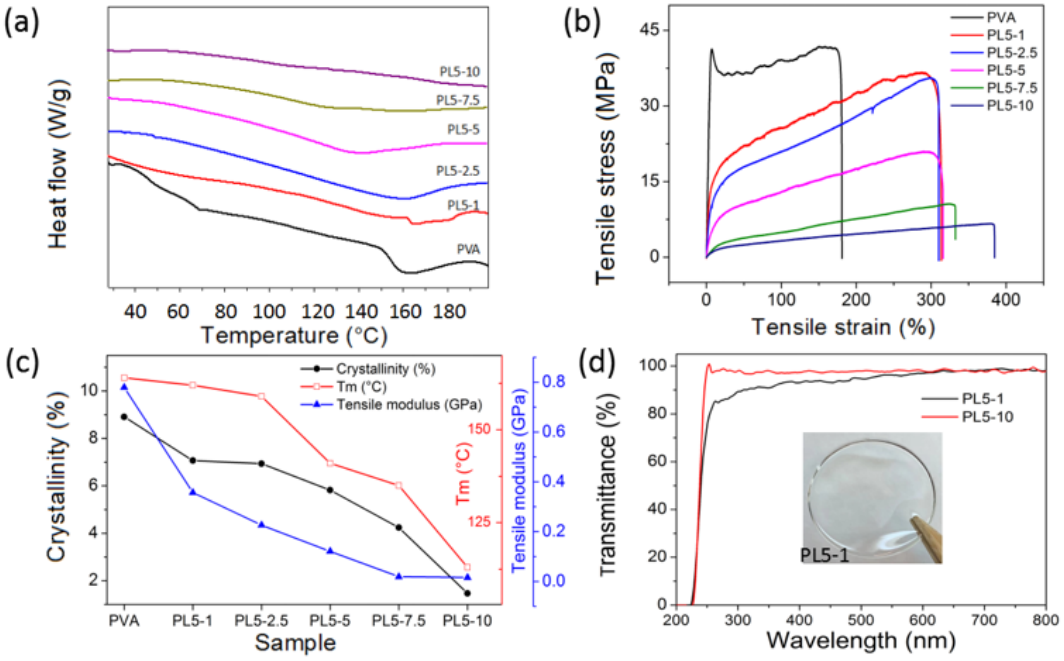

Figure 5. Thermal and tensile properties of the dehydrated PVA/IL electrolytes. (a) DSC and (b) tensile test results of dehydrated electrolytes; (c) the melting point, crystallinity, and tensile modulus of the PVA/IL electrolytes with different IL content; (d) UV-Vis spectra of PL5-1 and PL5-10 iEAP

(180%) are recorded in the PVA membrane. After loading the IL, the tensile results of the PVA/IL electrolytes are more or less similar to the elastic deformation characteristics of rubber, and the tensile strength and modulus decrease for higher IL content, while the elongation at the breaking point increasing significantly. The crystallinity of PL5-1 is decreased by less than 2% when compared to the PVA membranes, and the tensile modulus is decreased by 54.17% to 0.357 GPa. After setting the mass fraction between the PVA and IL at 1:2, the tensile modulus of PL5-10 had the smallest value (0.016 GPa). In addition, the breaking strength and elongation at the breaking point of PL5-1 and PL5-2.5 are comparable. When the IL content is very high (e.g. PL5-10), the elongation at the breaking point is improved by 383% because of the enhanced flexibility of the PVA after the self-assembly of IL at a higher content. Due to the good compatibility of IL and PVA, adding IL enhances the flexibility of the PVA/IL electrolyte membrane, thereby improving the elongation at the breaking point. However, the possible hydrogen bond formation between IL and PVA enhances the strength of the electrolyte. Therefore, the variation in elongation at break shown was not obvious at lower IL content (i.e., from PL5-1 to PL5-5). When the IL content further increases, the flexibility of the electrolyte substantially increases due to the self-assembly of IL at a higher content.

The crystallinity, melting point, and tensile modulus of the PVA/IL electrolytes in different samples are summarized in Figure 5(c). The crystallinity of the polymer is significantly reduced by loading IL. Therefore, the T_m and the tensile modulus of the electrolytes are inversely proportional to the IL content, respectively. Figure 5(d) shows the optical transmission of PL5-1 and PL5-10 electrolytes containing ~10 wt.% water. The IL used in this work is miscible and compatible with PVA even at higher concentrations (i.e. PL5-10). The resulting electrolytes are highly transparent in the visible spectrum, indicating good homogeneity of the materials [49]. Moreover, the optical transparency of the PL5-10 electrolyte increases within the wavelengths of 250 - 600 nm when compared to the PL5-1 electrolyte, due to the lower PVA crystallinity, as confirmed by the DSC results. The PVA/IL electrolytes with high transparency within the visible wavelength range of 400 - 750 nm were obtained for all compositions, demonstrating its promising potential as transparent actuators such as smart wipers [50]. They were used for the preparation of iEAP samples for subsequent bending performance assessment.

3.3 Bending performance of the PVA/IL iEAP in different IL contents

The PVA/IL electrolytes fabricated by solution casting naturally contain water owing to the hygroscopicity of C_{10}MIMCl. As shown in Figure 6, it was found that the IL absorbed water from the air with the water content up to 2.84 wt.% during the first week. Then, the absorption of water became slower in the following two weeks. The highest water content was 4.19 wt.%, and the water content remained at ~3.86 wt.% dynamically. This value is lower than the water content in the as-fabricated PVA/IL electrolytes (~12.22 wt.% of IL in PL5-1) because crystalline water is retained during the solution casting process [51]. Water is important to the electromechanical behavior of iEAPs, both in this work as well as in classical studies. In our work, the performance of the iEAPs can be improved by the presence of retained water after the casting process of the PVA/IL electrolytes. In addition, the water content in the PVA/IL iEAPs is tunable through the absorption of water by IL in the environment.

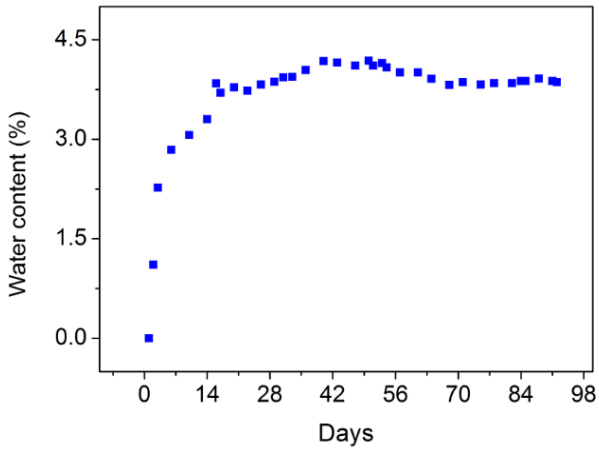

Figure 6. The water content in C_{10}MIMCl as a function of time

Here, we firstly investigated how the IL content affects the actuation performance of iEAPs by adjusting the water content in all electrolytes to similar levels (~10 wt.%, as shown in Table 1), ascribed to the hygroscopicity of IL and crystalline water [51]. The electrochemical behaviour, tensile property, and bending performance of different iEAPs are shown in Figure 7. The three-layered iEAPs can be regarded as parallel-plate capacitors, where the mobile ions only migrate within the electrolyte and no electrochemical reactions are involved [52, 53]. The dynamics of the cations ($C_{10}MIM^+$) are restricted on the PVA chains with the help of the hydrogen bonds, however, the anions (Cl^-) are free to migrate under an electric field. When a voltage is applied to the PVA/IL iEAP, the Cl^- ions in the electrolyte redistribute, forming an electric double layer at the interfaces between the electrode and electrolyte.

Figure 7(a) shows the CV loops of the iEAPs with similar water levels (~10 wt.%) but different IL content. The CV loops are all symmetrically closed. This indicates that the gold electrodes are symmetric and have strong interfacial bonding with the electrolytes. The iEAPs, except for PL5-5, show neither the rectangular shape of an ideal capacitor nor pronounced peaks. This is attributed to the solution resistance and interfacial polarizations, evidenced by the inclined and narrow loop. A higher current response indicates a higher capacitance of the iEAP, which corresponds to a higher electromechanical response under the same voltage stimulus. In the CV loop of PL5-5, the current increases with voltage up to 0.2V. However, the current is reduced if the applied voltage is above 0.2V. This is due to the spontaneous adsorption of ions by hydrophilic functional groups in the polymer with a new interface [54]. When a large number of ions accumulate at the electrode-electrolyte interface, a higher capacitance is obtained. However, a high IL content does not guarantee a high capacitance. The neutral molecules formed by the self-assembled IL are polarized under an electric field and presumably affect the charge accumulation in the electrodes. In addition, the migration of ions is minimized because of the reinforced ionic interaction. Figure 7(b) shows the tensile strain

of the electrolytes. Compared with the dehydrated electrolytes, the tensile modulus of electrolytes after absorbing water is decreased as shown in Figure 7(d), but the elongation at the breaking point shows an opposite response. This is because water molecules occupy more space between the polymeric chains which reduces the intermolecular forces.

The deformation responses of the iEAPs at 2V DC are shown in Figure 7(c-e). Although the authors in other reports state that the direction of deformation depends on the radius of the ions [18, 55], all PVA/IL iEAPs contained ~10 wt.% water bend towards their cathode sides, indicating anion-controlled deformations. This is consistent with the ATR-FTIR results. The iEAP sample with the highest capacitance, PL5-5, shows the most obvious deformation along the entire length. The highest curvature appears near the contact electrode, up to 19.38 m^{-1}. The curvatures of all iEAPs show a downward trend along the length due to the resistance of the electrolyte and electrode [37]. For PL5-2.5 and PL5-7.5, their CV patterns are similar but the latter shows a stronger current response during charging. However, the excess IL in PL5-7.5 hinders the migration of the Cl^- ions, resulting in a less noticeable curvature profile, with the curvature at its tip (4.07 m^{-1}) smaller than that of PL5-2.5 (9.26 m^{-1}). In contrast, the deformation response of PL5-10 at the highest IL content shows the weakest average curvature of 2.66±0.05 m^{-1}.

The capacitance, mechanics, and average curvature of these iEAPs are summarized in Figure 7(d). The average curvature for each composition is also listed in Table 2. The electromechanical response of iEAP follows the variation law of capacitance. When the IL content is low enough, it dissociates into the water completely which increases the concentration of chloride ions and improves the flexibility of the samples. Therefore, the bending response is controllable via monitoring the IL content. The highest average curvature of 17.45±0.41 m^{-1} is observed in PL5-5. However, the interionic force is proportional to the IL content. Although the flexibility of the iEAP is enhanced, the mobile ions struggle to migrate in the electrolyte. In addition, the polarized IL molecules in the intra-electrolyte diffusion layer would contribute less significantly to bending, resulting in weakening the bending performance of PL5-7.5 and PL5-10 iEAPs.

3.4 Bending performance of iEAPs made up of PL5-5 electrolyte at various water content

The water-soluble and hydrophilic properties of the C_{10}MIMCl are advantageous in forming uniform membranes, using the casting method in combination with the PVA matrix. However, the strong interaction [28] between the cation and anion in C_{10}MIMCl limits the rate of dissociation and ion migration, especially for the anhydrous PVA/IL-based iEAP. Among the anhydrous iEAPs, only PL5-5 shows a

Table 2. Summary of average curvature for iEAP samples with different IL and water content.

iEAPs with different IL content					
Sample	**PL5-1**	**PL5-2.5**	**PL5-5**	**PL5-7.5**	**PL5-10**
Average curvature (m^{-1})	6.29±0.24	10.76±0.44	17.45±0.41	5.95±0.20	2.66±0.05

PL5-5 iEAPs with different water content					
Sample	**PL5-5-0**	**PL5-5-5.76**	**PL5-5-10.14**	**PL5-5-14.96**	**PL5-5-19.80**
Average curvature (m^{-1})	5.17±0.13	12.15±0.15	17.45±0.41	29.35±0.27	40.53±0.21

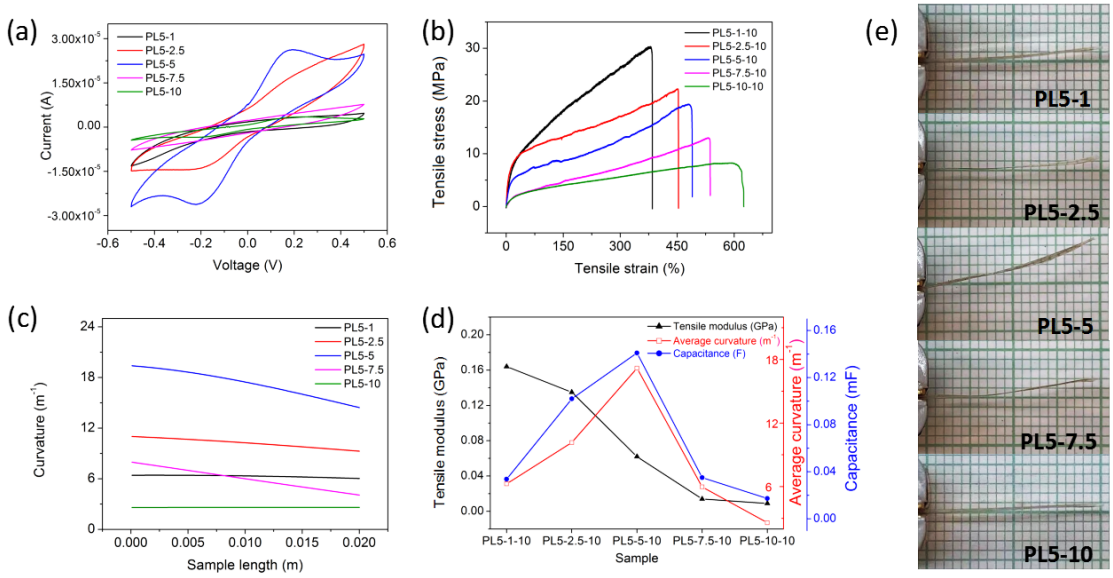

Figure 7. Comparison of the (a) CV loops, (b) tensile test, (c, d) bending performance, and (e) deflection images of the iEAPs in different IL concentrations and same water content

noticeable deformation at 2V DC with an average curvature of 5.23 m^{-1}, and is attributed to the high flexibility of the PL5-5 iEAP associated with migratable ions. In the section 3.3, the hydrated (10.14 wt.% water) PL5-5 exhibits the highest capacitance and the desired actuation performance when compared to other electrolytes with the equivalent water content.

As shown in Figure 8(a), in the presence of water, the current response of PL5-5 subjected to the same input triangular voltage is stronger because the solution resistance in the electrolyte is decreased, as evidenced by the wider CV loop. After vacuum drying, the CV loop of the iEAP is almost flattened, with a capacitance of only 0.018 mF. Under the defined experimental conditions, the maximum attainable water content for the sample PL5-5 is limited to 19.80 wt.%. After the water content is increased to 19.80 wt.%, the corresponding capacitance increases significantly to 0.315 mF, which is over 17 times higher than that of the anhydrous sample. In addition, the rate of dissociation in IL increases when the PL5-5 electrolyte absorbs water which provides additional channels for ions migration. This forms a thicker double electric layer to improve the bending response. The increase in water content may also soften the interaction between the PVA chains, which always makes the electrolytes more flexible. After absorbing 5.76 wt.% water, the tensile modulus of PL5-5 decreases from 0.121 GPa to 0.064 GPa rapidly, as shown in Figure 8(b). When the water content reaches 19.80 wt.%, the tensile modulus of the sample drops to 0.010 GPa only. The bending performance of PL5-5 iEAPs with different water content at 2V DC is shown in Figure 8(c-e). The average curvature of each sample at a particular water content is listed in Table 2. With a higher water content in the iEAP, the bending curvature is more noticeable. Despite the curvature of PL5-5-0 at $\boldsymbol{L = 0}$ being 5.31 m^{-1}, PL5-5-19.80 shows the highest curvature of 62.37 m^{-1} at the same position. Similarly, these iEAPs exhibit anion-controlled deformation towards the cathode, in which the bending curvature decays along the longitudinal axis of the sample. From the above result, the iEAP shows enhanced performance when the water content due to moisture absorption increases. The actuation performance of iEAP depends on the amount of its internal movable ions, and higher water content is conducive to the migration of chloride ions and improve the flexibility of electrolytes, which leads to a more considerable actuation performance. Therefore, it is expected that, theoretically, further increases in water content may enhance the average curvature of the samples. In a drier environment, the water in the actuator will slowly evaporate to a lower level, affecting the actuation. Therefore, it has great potential as an environmental-adaptive device in response to environmental humidity. Figure 8(f) shows the fast response time and the actuation reversibility of the PL5-5-19.80 iEAP. The PL5-5-19.80 iEAP responds within 1 s under the 2V DC stimulation. After removing the electric potential, the iEAP returns to its undeformed state within 50 s.

Table S1 summarizes other work for iEAPs containing imidazolium IL, including their compositions and performance. It has been reported that the bending displacement of an iEAP using PVDF/C_{10}MIMCl electrolyte was less than 0.5 mm, corresponding to an average curvature of ~1.00 m^{-1} [13]. In comparison, the lowest

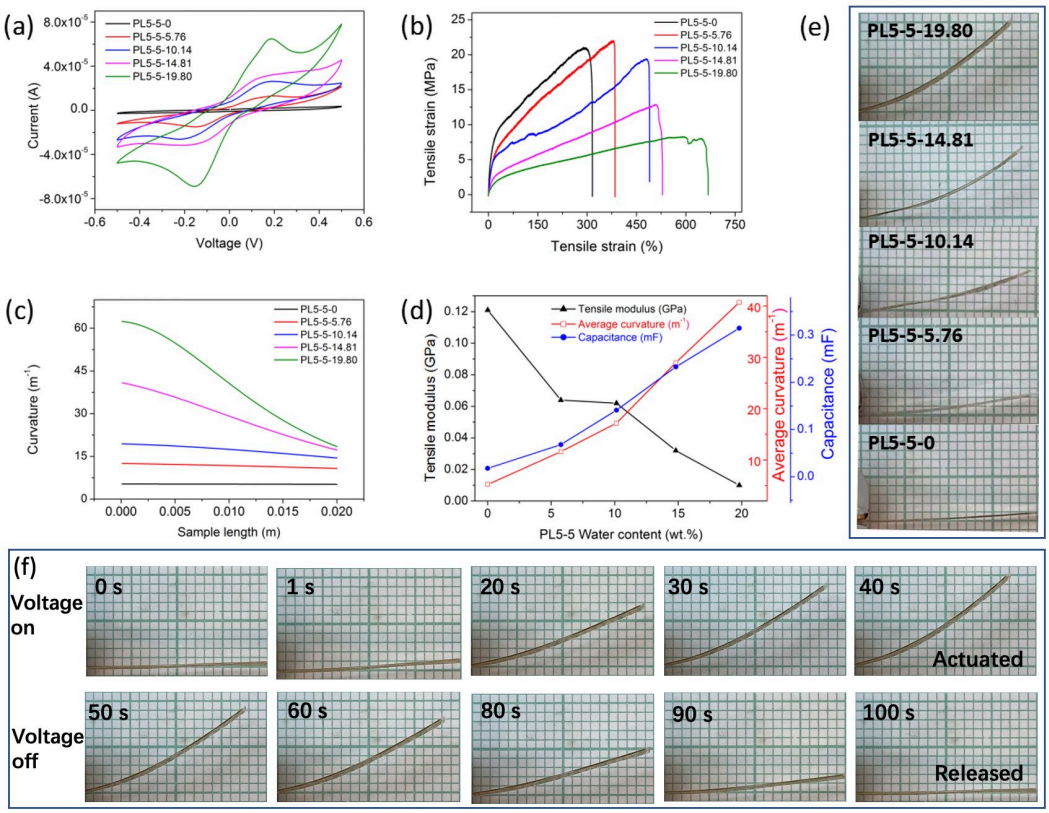

Figure 8. Comparison of the (a) CV loops, (b) tensile test, (c, d) bending performance, (e) deflection images of different iEAP (PL5-5) samples with various water content, and (f) images show the fast response time and actuation reversibility of iEAP (PL5-5-19.80)

performing iEAP in our work, i.e. the dehydrated PL5-5 iEAP, showed over four times improvement in the average curvature (5.17±0.13 m^{-1}). Furthermore, an iEAP containing 1-butyl-3-methylimidazolium chloride (C_4MIMCl), which is an IL with shorter alkyl chains compared with C_{10}MIMCl, was reported with an average curvature of 5.06 m^{-1} [56]. The average curvature of the PL5-5-19.80 iEAP is improved by over seven times, reaching 40.53±0.21 m^{-1}. Bae et al. [57] reported an iEAP prepared by exchanging 1-ethyl-3-methylimidazolium trifluoromethanesulfonate (IL) had the highest curvature of 3.82 m^{-1} at 2.5 V. This is an anhydrous iEAP with the mobile ion C_2MIM^+, which is larger than Cl^-. Compared to their work, our PVA/IL iEAPs showed improvement for more than 35.3%.

The water content in the PL5-7.5 and PL5-10 samples can reach as high as 30 wt.% because of the hygroscopicity of IL and the formation of crystalline water [51] during the casting process. It is interesting to note that with higher water content, the direction of the deflection for PL5-7.5 and PL5-10 iEAPs is changed and opposite to the other samples, i.e. towards the anode side, under the same stimulation conditions. We hypothesize that this is due to the re-dissociation of neutral IL molecules in the samples thereby allowing more ions to migrate across the electrolytes at high moisture levels. In this case, the anions and cations move toward the anode and cathode of the iEAP accordingly, and the deformation arises from the volumetric difference between the smaller anions (Cl^-) and the much larger cations ($C_{10}MIM^+$). Further study is needed in exploring the detailed mechanism that results in such a different manner to other iEAP samples.

Despite the great improvement in the electromechanical behaviour, failure of PVA/IL iEAPs is inevitable owing to the fatigue and cracking of the metal electrodes during bending, or possible physical damage of the electrolytes. This problem can be solved by using transparent conductive polymer thin film electrodes, such as PEDOT, to improve the cycle life of the iEAPs [4]. Moreover, introducing self-healing properties to the materials can be another promising strategy. For example, the self-healing function can be achieved by using liquid metal composites as electrodes [58, 59]. Additionally, it has been reported that PVA is also a promising self-healing material, based on the principle of reversible dynamic chemical bonds [60]. Thus, the self-healing function of iEAPs could be achievable using the PVA/IL electrolyte developed in this study. Moreover, capacitive sensing using the PVA/IL electrolyte is also possible because of the uneven distribution of ions when stimulation is applied [61]. Utilizing this property, a dual actuating and self-sensing iEAP could be realized by designing and generating an additional sensing circuit [53]. Finally, it is foreseeable that by formulating printable PVA/IL ink, 3D layer-by-layer printing technologies such as fused deposition modelling [62] and laser printing [63] can be employed in producing iEAPs with more complex electromechanical responses as well as addressing multiple operating environments demands.

4 Conclusions

Highly transparent electrolytes composed of PVA and C_{10}MIMCl were prepared. The electrolytes have overcome the poor deformation in iEAP using IL containing long alkyl chains. The interaction between the polymer and IL has been analysed and meanwhile, the crystallization, mechanical, and electrochemical properties related to the hygroscopicity of IL were studied. The formation of hydrogen bonding between the PVA and the imidazole ring was confirmed by ATR-FTIR spectroscopy, facilitating the transfer of anions within the electrolytes. The iEAPs are fabricated by sandwiching the PVA/IL electrolytes between two gold electrodes. They bend towards the cathode due to the immobilization of the cations in IL by hydrogen bonding, leaving Cl^- as the mobile ions for generating deformation. The bending performance was calculated by the curvature profile and the average curvature of the iEAPs. We confirm that the bending performance is related to the IL and water content in the electrolyte and electric double-layer capacitance. Under a DC of 2V, the highest average curvature (40.53±0.21 m^{-1}) occurs in the PL5-5 sample with a water content of 19.80 wt.%. Our work also shows the potential to design programmable and transparent actuators and sensors through external connections to microcontrollers or microprocessors.

Author Contributions

Chak-Yin Tang: Conceptualization, Supervision, Methodology, Project Administration, Writing – review & editing. Yuqing Dong: Methodology, Investigation, Analysis, Writing – original, Writing – review & editing. Ka-Wai Yeung: Methodology, Investigation, Analysis, Writing – original, Writing – review & editing. Chi Ho Wong: Writing – review & editing. Wing-Cheung Law: Supervision, Methodology, Writing – review & editing. Gary Chi-Pong Tsui: Writing – review & editing. Xiaolin Xie: Methodology, Writing – review & editing.

Conflicts of interest

The authors declare that they have no known competing financial interests or personal relationships that could have appeared to influence the work reported in this paper.

Acknowledgements

The work described in this paper was fully supported by a grant from the Research Grants Council of the Hong Kong Special Administrative Region, China (Project No. PolyU 15200318).

Notes and references

1 Panwar, V., Gopinathan, A., J. Mater. Chem. C., 2019, 7(30), 9389-9397.
2 Li, Y., Guo, M., Li, Y., J. Mater. Chem. C., 2019, 7(42), 12991-13009.
3 Panwar, V., Anoop, G. J., Mater. Chem. C., 2018, *6*(31), 8395-8404.
4 D. Guo, L. Wang, X. Wang, Y. Xiao, C. Wang, L. Chen, et al., Sens. Actuators B Chem., 305(2020), pp. 127488.
5 He, Y., Wu, J., Lin, M., Xiao, S., Liu, H., Zhou, P., J. Mater. Chem. C., 2021, *9*(46), 16378-16390.
6 N. Terasawa, Sens. Actuators B Chem., 2018, 257, 815-819.
7 Y.J. Tang, Z.G. Xue, X.P. Zhou, X.L. Xie, C.Y. Tang, Sens. Actuators B Chem., 2014, 202, 1164-1174.
8 Y.Q. Dong, K.W. Yeung, C.Y. Tang, W.C. Law, G.C.P. Tsui, X.L. Xie, Nanotechnol. Rev., 2021, 10, 99-116
9 D. Guo, Y. Han, J. Huang, E. Meng, L. Ma, H. Zhang, et al., ACS Appl. Mater. Interfaces, 2019, 11, 2386-97.

10 F. Wang, Y. Kong, F.F. Shen, Y.F. Wang, D.H. Wang, Q.C. Li, Compos. B. Eng., 2022, 228, 109436.
11 B.T. White, T.E. Long, Macromol. Rapid Commun., 2019, 40, 1800521.
12 D.M. Correria, L.C. Fernandes, P.M. Martins, C.G. Astrain, C.M. Costa, J. Reguera, S.L. Méndez, Adv. Funct. Mater., 2020, 30, 1909736.
13 R. Mejri, J. Dias, S.B. Hentati, G. Botelho, J. Esperança, C. Costa, et al., Eur. Polym. J., 2016, 85, 445-51.
14 R. Mejri, J.C. Dias, A.C. Lopes, S.B. Hentati, M.M. Silva, G. Botelho, A. Mão de Ferro, J.M.S.S. Esperança, A. Maceiras, J.M. Laza, J.L. Vilas, L.M. León, S.L. Mendez, Eur. Polym. J., 2015, 71, 304-313.
15 M. Safari, L. Naji, R.T. Baker, F.A. Taromi, Polym., 2015, 76, 140-9.
16 Y. Liu, S. Liu, J. Lin, D. Wang, V. Jain, R. Montazami, Appl. Phys. Lett., 2010, 96, 223503.
17 D.M. Correia, J.C. Barbosa, C.M. Costa, P.M. Reis, J.M.S.S. Esperança, V. de Zea Bermudez, S. L. Méndez, J. Phys. Chem. C, 2019, 123, 12744-12752.
18 L. Yang, D. Zhang, H. Wang, X. Zhang, Adv. Eng. Mater., 2020, 22, 2000537.
19 S. Nemat-Nasser, Y. Wu, J. Appl. Phys., 2003, 93, 5255-67.
20 Y. Cha, M. Porfiri, J. Mech. Phys. Solids, 2014, 71, 156-78.
21 V. Panwar, K. Cha, J.O. Park, S. Park, Sens. Actuators B Chem., 2012, 161, 460-70.
22 A. Khan, R. Jain, M. Naushad, Smart Mater. Struct., 2015, 24, 095003.
23 R.K. Jain, Soft Robot. Rehabilit., Elsevier2021, pp. 39-87.
24 C.Y. Wong, W.Y, Wong, K.S. Loh, K.L. Lim, React. Funct. Polym., 2022, 171, 105160.
25 O. Kim, S.J. Kim, M.J. Park, Chem. Commun., 2018, 54, 4895-904.
26 M. Zhang, M. Wang, X. Zhang, C. Zhang, M. Li, S. Yu, Sens. Actuators B Chem., 2022, 356, 131319.
27 A. Kesküla, A.L. Peikolainen, R. Kiefer, T. Tamm, Synth. Met., 2020, 268, 116502.
28 P.A. Hunt, B. Kirchner, T. Welton, Chem. Eur. J., 2006, 12, 6762-75.
29 S. De Sarkar, S. Mitra, S.K. Ghosh, Eur. Phys. J. E, 2020, 43, 1-10.
30 S. Cuadrado-Prado, M. Dominguez-Perez, E. Rilo, S. García-Garabal, L. Segade, C. Franjo, O. Cabeza., Fluid phase Equilib., 2009, 278, 36-40.
31 T. Myrdek, C. Popescu, W. Kunz, J. Mol. Liq., 2021, 322, 114947.
32 E.S. Marín Cardona, J. Rojas Camargo, Y.A. Ciro Monsalve, African Journal of Pharmacy and Pharmacology, 2014, 8, 674-684.
33 N.A. Peppas, E.W. Merrill, J. Appl. Polym. Sci., 1976, 20, 1457-65.
34 Z.Z. Sun, L. Yang, D. Zhang, W.L. Song, Sens. Actuators B Chem., 2019, 283, 579-589.
35 C. Lu, L. Zhao, Y. Hu, W. Chen, Chem.l Commun., 2018, 54, 8733-6.
36 L. Yang, Z. Sun, F. Li, S. Du, W. Song, Appl. Phys. A, 2019, 125, 1-15.
37 Y. Dong, K.W. Yeung, W.C. Law, G.C.P. Tsui, X. Xie, C.Y. Tang, Polym. Test., 2022, 106, 107463.
38 C.W. Liew, S. Ramesh, A. Arof, Int. J. hydrog. Energy, 2014, 39, 2917-28.
39 P.K. Singh, B. Bhattacharya, R. Nagarale, K.W. Kim, H.W. Rhee, Synth. Met., 2010, 160, 139-42.
40 M. Vraneš, A. Tot, S. Armaković, S. Armaković, S. Gadžurić, J. Chem. Thermodyn., 2016, 95, 174-9.
41 G. Chen, N. Chen, Q. Wang, Mater. Des., 2018, 157, 273-83.
42 G.B. Thorat, S. Gupta, Z. Murthy, Chin. J. Chem. Eng., 2017, 25, 1402-11.
43 Y. Lu, D. Wang, T. Li, X. Zhao, Y. Cao, H. Yang, Y.Y. Duan, Biomater., 2009, 30, 4143-51.
44 H.S. Mansur, C.M. Sadahira, A.N. Souza, A.A. Mansur, Mater. Sci. Eng. C, 2008, 28, 539-48.
45 J.P. Canal, T. Ramnial, D.A. Dickie, J.A. Clyburne, Chem. Commun., 2006, 1809-18.
46 G. Chen, N. Chen, L. Li, Q. Wang, W. Duan, Ind. Eng. Chem. Res., 2018, 57, 5472-81.
47 A. Saroj, S. Chaurasia, S. Kataria, R. Singh, Phase Transit., 2016, 89, 578-97.
48 A. Saroj, S. Krishnamoorthi, R. Singh, J. Non Cryst. Solids, 2017, 473, 87-95.
49 H. Okuzaki, S. Takagi, F. Hishiki, R. Tanigawa, Sens. Actuators B Chem., 2014, 194, 59-63.
50 L. Chen, M. Zhang, W. Zhang, Z. Zhou, Y. Zhou, D. Xia, J. Li, Z. Huang, C. Liu, S. Fan, Nanoscale, 2016, 8, 6877-6883.
51 Y. Ishii, N. Matubayasi, G. Watanabe, T. Kato, H. Washizu, Sci. Adv., 2021, 7, eabf0669.
52 L. Yang, D. Zhang, X. Zhang, A. Tian, J. Mater. Res., 2021, 36, 1295-305.
53 W. MohdIsa, A. Hunt, S.H. HosseinNia, Sensors, 2019, 19, 3967.
54 K.P.S. Hussan, M.S. Thayyil, T.V. Jinitha, K. Jayant, J. Mol. Liq., 2019, 274, 402-413.
55 T. Fukushima, K. Asaka, A. Kosaka, T. Aida, Angew. Chem. Int. Ed., 2005, 44, 2410-3.
56 R. Gonçalves, K. Tozzi, M. Saccardo, A. Zuquello, C. Scuracchio, J Solid State Electrochem., 2020, 24,1845-56.
57 Y. Bae, M. Park, M. Kim, S. Hwang, S. Kim, M. Jeon, Thin Solid Films, 698(2020), pp. 136848.
58 Z.H. He, S.S. Jiao, Z.P. Wang, Y.F. Wang, M.Y. Yang, Y. Zhang, Y.W. Liu, Y.Z. Wu, J. Shang, Q.M. Chen, R.W. Li, ACS Appl. Mater. Interfaces, 2022, 14, 14630-14639.
59 Z.X. Zhou, C.H. Qian, W.Z. Yuan, Compos. Sci. Technol. 2021, 203, 108608.
60 J.Y. Ai, K. Li, J.B, Li, F. Yu, J. Ma, Int. J Biol. Macromol., 2021, 172, 66-73.
61 Y.J. Wang, G.Q. Tang, C. Zhao, K.L. Wang, J.L. Wang, J. Ru, J.J. Sheng, L.F. Chang, L.J. Li, Sens. Actuators B Chem., 2021, 345, 130421.
62 G. Matijašić, M. Gretić, J. Vinčić, A. Poropat, L. Cuculić, T. Rahelić, J. Drug Deliv. Sci. Technol., 2019, 52, 677-686.
63 P. Fei, J.Y. Jia, S.P. Peng, W.J. Yang, S.Z. Bin, C.J. Shuai, Virtual Phys. Prototyp., 2020, 15, 211-226.

Supplementary Information

Preparation and Characterization of Transparent Polymeric Electrolyte Containing Ionic Liquid with Long Alkyl Chains for Electroactive Polymers

Yuqing Dong[a], Ka-Wai Yeung[a], Chak-Yin Tang[a*], Chi Ho Wong[a], Wing-Cheung Law[a], Gary Chi-Pong Tsui[a], Xiaolin Xie[b]

[a] *Department of Industrial and Systems Engineering, The Hong Kong Polytechnic University, Hong Kong, China*

[b] *School of Chemistry and Chemical Engineering, Huazhong University of Science and Technology, Wuhan, Hubei 430074, China*

* Corresponding authors

Email address: cy.tang@polyu.edu.hk (Chak Yin Tang), Phone: +852 2766 6608, Fax: + 852 2362 5267

Postal address: Department of Industrial and Systems Engineering, The Hong Kong Polytechnic University, Hung Hom, Kowloon, Hong Kong, China.

1. Performance comparison of iEAPs containing IL

We found that water plays a major role in the actuation performance of the PVA/IL-based iEAPs. For the dehydrated iEAP samples, no obvious deformation was observed (except for PL5-5), due to the constraints of the high viscosity, the large molecular size of C_{10}MIMCl, and a small actuation voltage (2V). The deformation comparison of IL contained iEAPs is summarized in Table S1. The structures of materials in Table S1 are shown in Figure S1.

Table S1. Performance comparison of typical IL-containing iEAPs

Electrolyte composition	Mobile ion	Bending direction	Actuation voltage (V)	Average curvature (m^{-1})	Reference
PVDF/ $C_{10}MIMCl$	$C_{10}MIM^+$ & Cl^-	anode	10	~1.00	[1]
Nafion/ C_4MIMCl	C_4MIM^+	anode	4	~5.06	[2]
Nafion/ C_2MIMTf	C_2MIM^+	anode	2.5	3.82	[3]
BC/C_2MIMBF_4	C_2MIM^+	anode	1	~6.60	[4]
BC/ C_2MIMBF_4/MWCNT	C_2MIM^+	anode	1	~12.50	[4]
			1.5	16.47	
Cellulose/ C_4MIMCl	Cl^-	cathode	2	~4.42	[5]
			5	~24.95	
Nafion/LiCl/ C_2MIMBF_4	Li^+& C_2MIM^+	anode	2	~15.13	[6]
Nafion/ C_2MIMBF_4	C_2MIM^+			~2.66	
Nafion/ C_2MIMBF_4	C_2MIM^+	anode	2	~2.15	[7]
Nafion/ C_4MIMCl	C_2MIM^+	anode	2	~2.44	[8]
			5	~9.89	
CBC/ C_2MIMBF_4/MWCNT	C_2MIM^+ & BF_4^-	anode	1	12.05	[9]
MFC/ C_2MIMBF_4	C_2MIM^+ & BF_4^-	anode	2	12.40	[10]
CA/ C_4MIMBF_4/GN	C_4MIM^+ & BF_4^-	anode	3	14.18	[11]
PL5-5-0	Cl^-	cathode	2	5.17	this work
PL5-5-19.80				40.53	

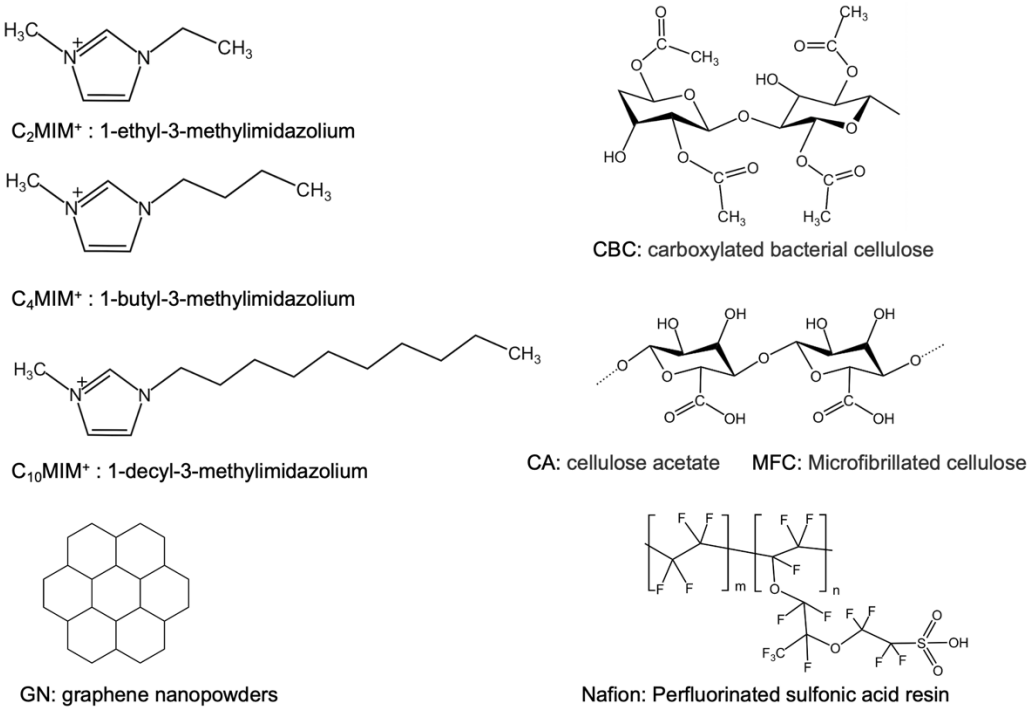

Figure S1. Structures of IL cations, filler, and polymer matrix

References

[1] R. Mejri, J. Dias, S.B. Hentati, G. Botelho, J. Esperança, C. Costa, S Lanceros-Mendez, Eur. Polym. J., 2016, 85, 445-51.

[2] R. Gonçalves, K. Tozzi, M. Saccardo, A. Zuquello, C. Scuracchio, J Solid State Electrochem., 2020, 24, 1845-56.

[3] Y. Bae, M. Park, M. Kim, S. Hwang, S. Kim, M. Jeon, Thin Solid Films, 2020, 698, 136848.

[4] Y.F. Wang, F. Wang, Y. Kong, L. Wang, Q.C. Li, Smart Mater. Struct., 2022, 31, 025023

[5] Z.Z. Sun, L. Yang, D. Zhang, W.L. Song, Sens. Actuators B Chem., 2019, 283, 579-589.

[6] Lee, S., Hwang, L., Lee, J. Y., Yang, T., Jho, J. Y., Park, J. H., Sens. Actuators B Chem., 2022, 372, 132616.

[7] Wang, H. S., Cho, J., Park, H. W., Jho, J. Y., Park, J. H., J. Ind. Eng. Chem., 2021, 96, 194-201.

[8] Tozzi, K. A., Gonçalves, R., Barbosa, R., Saccardo, M. C., Zuquello, A., Sgreccia,

E., di Vona, M. L., J. Appl. Electrochem., 2022, 1-15.

[9] Wang, F., Wang, L., Wang, Y., Wang, D., Appl. Phys. A, 2022, 128(10), 1-12.

[10] Wang, F., Kong, Y., Shen, F., Wang, Y., Wang, D., Li, Q., Compos. Part B-Eng., 2022, 228, 109436.

[11] Nan, M., Wang, F., Kim, S., Li, H., Jin, Z., Bang, D., Choi, E., Sens. Actuators B Chem., 2019, 301, 127127.